Phase-Only Tapers for Regular Planar Arrays, a Heuristic Nonlinear-FM Approach

Jeffrey O. Coleman
http://alum.mit.edu/www/jeffc

Dan P. Scholnik
dan.scholnik@nrl.navy.mil

Kelly R. McPhail*
kelly.mcphail@ll.mit.edu

Naval Research Laboratory
Radar Division, Code 5328
Washington DC, USA

MIT Lincoln Laboratory
Lexington MA, USA

Abstract—*We present a simple approach to constructing phase-only tapers for regular planar arrays that is analogous to the instantaneous-frequency approach classically used to construct FM-chirp waveforms with high time-bandwidth products. Design experiments for a large triangular-grid array show that the crude results yielded by this method when aperture-beamwidth products are modest can sometimes be "tweaked" into reasonableness. We conjecture that such a taper would improve upon the usual uniform-weight starting point for a nonlinear-optimization approach that seeks out a local optimum. Specific design examples presented here nominally aim to approximate a brick-wall beam and a variant of a Gaussian beam.*

1. INTRODUCTION

We consider a narrowband planar phased array with elements laid out on a point lattice and with guard elements as necessary to ensure that the far-field array pattern factors into an embedded element pattern and an array factor. Mathematically, that array factor is the 2D Fourier transform of the array taper constructed as impulses at the element locations with areas given by the complex element weights. Phase-only tapers, those with all complex weight magnitudes strictly identical, are desirable in active radar transmit arrays simply to maximize radiated power when individual-element power capability is the limiting factor. The simplest phase-only taper, uniform illumination, is widely used for pencil beams in radar systems. Designing phase-only tapers for broader beams, however, is notoriously difficult.

Amplitude-only tapers associate a real (and positive in most cases) weight with each element and are readily designed using convex optimization [1]. A design problem cast as minimizing a linear or positive-definite quadratic objective subject to design constraints is convex if (and only if) given any two tapers $h_{\mathbf{n}}$ and $g_{\mathbf{n}}$ individually satisfying those design constraints, any taper $\alpha h_{\mathbf{n}} + (1-\alpha) g_{\mathbf{n}}$ having $0 \leq \alpha \leq 1$ to interpolate between them satisfies those constraints as well. Convexity guarantees a single local optimum, which therefore is actually global, and numerical convex solvers with the power to handle large 2D tapers are readily available [2]. The situation is not materially different for combined amplitude and phase tapers, which assign a complex weight to each element. The number of real variables in the convex optimization doubles, but the principles are the same.

A phase-only taper is quite different. Because it gives all complex weights the same magnitude, many nonconvex constraints of the form $|h_n|=1$ (to pick a particular magnitude) result. The resulting nonconvex optimization problem is generally plagued with a vast, even ghastly number of local optima. Research experience suggests that for large arrays there is no reliable way of discovering which of these local optima is the global one. Viable phase-only design strategies then tend to either use a heuristic method to pick a reasonable suboptimal design or to use a preliminary design chosen in that way to initialize a follow-on optimal search for a nearby local optimum. Whether such a procedure is useful depends on the particulars.

Examples of 1D heuristic design approaches can be found in [3], [4], [5], [6], [7]. Reference [8], which proposes separate beams on interlaced subarrays, represents a 2D heuristic method. Local optimization approaches are presented for the 1D problem in [9], [10], [11], [12], [13] and for 2D in [14], [15]. Some of those local-optimization methods are combined with heuristic strategies, such as slowly walking the design parameters out from a uniform-illumination starting point, re-optimizing at each step. As might be expected, local solutions typically have a markedly worse tradeoff between mainbeam and sidelobe performance than non-phase-only designs. The complicated nature of the error surface generally makes it difficult to determine for a particular design whether this is due to the phase-only constraint or to a poor local minimum. Nonlocal optimization methods such as simulated annealing and genetic algorithms have also been

*K. R. McPhail was with the Naval Research Laboratory, Radar Division, Code 5327 when this work was done.

Work supported by the Naval Research Laboratory base program.
This is Array 2010 paper number 367.

used in 1D and 2D [16], although they do not guarantee a global solution either. There are also hybrid approaches [17] that locally optimize the coefficients of a small number of heuristically chosen phase basis functions.

1.1 This paper's approach

One common heuristic approach for uniform line arrays in 1D borrows from the classical design of FM-chirp waveforms for radar [18]. Stationary-phase mathematics are typically offered in justification, but the core idea is simply to hope that the magnitude of the Fourier spectrum at a given frequency f is proportional to the amount of time the instantaneous frequency, given for signal $\mathrm{e}^{\mathrm{j}\theta(t)}$ by $f_{\text{inst}}(t) = \frac{1}{2\pi}\frac{d\theta(t)}{dt}$, spends near f. It's very much like an integration change of variable $f = f_{\text{inst}}(t)$ or $t = f_{\text{inst}}^{-1}(f)$ so that $dt = \frac{df_{\text{inst}}^{-1}(f)}{df}\,df$. The signal spends time dt between instantaneous frequencies f and $f + df$, so we might hope that the Fourier spectrum will have magnitude at least roughly proportional to $\left|\frac{df_{\text{inst}}^{-1}(f)}{df}\right|$. Generally the messy part mathematically is dealing with the inverse-function aspect of this, but there are classic cases in which the relationships are not difficult to work out, and exploring them brings out the limitations of the approach.

For example, for $t \in \left(-\frac{T}{2}, \frac{T}{2}\right)$ the FM chirp signal

$$h(t) = \begin{cases} \mathrm{e}^{j\pi(Wt)(t/T)} & \text{for } |t| < T/2, \\ 0 & \text{otherwise.} \end{cases}$$

has instantaneous frequency Wt/T, which sweeps at a constant rate across interval $\left(-\frac{W}{2}, \frac{W}{2}\right)$ as t increases. One might hope then that its Fourier magnitude spectrum is roughly constant on that interval and zero elsewhere. In fact it is approximately so when, but only when, time-bandwidth product WT is large. In that case,

$$|H(f)| \approx \begin{cases} \text{some constant} & \text{for } |f| < W/2, \\ 0 & \text{otherwise.} \end{cases}$$

The purpose of this paper is to extend this simple 1D approach to 2D, to experiment with it computationally using a large triangular-grid array as a vehicle, and to demonstrate through hand-tweaked design examples that at least for some parameter combinations it is possible to obtain beams significantly broader than that resulting from uniform illumination and with perhaps tolerable in-beam ripple levels and sidelobe levels. In several cases the latter turn out to be significantly better than are obtained by typical local-optimization approaches and are sufficiently reasonable to encourage the use of such hand-tweaked beams as perhaps better starting points for local optimization. Such optimization is beyond the scope of this exploratory effort, but we hope other researchers will explore along these lines.

Section 2 walks through examples of increasing complexity, presenting computational results along the way. The computational design examples are for a narrowband planar array on an equilateral triangular grid with $\lambda/\sqrt{3}$ spacing. The array's 4507 elements have centers at those lattice points lying no more than $\sqrt{1237/3}\,\lambda$ from the origin. The approach explored obtains the phase weights by sampling a continuous distribution, so the key ideas would apply equally well to arrays on the square grid. The computational results, however, are specific to the particular array considered, as quantization effects appear quite significant, particularly at the array edges. We intend in [19] to expand upon the set of design examples presented here.

2. Sampled 2D FM chirps

2.1 A reference plot establishes the format

Designs will be presented in the format of Fig. 1, which shows the array factor resulting from uniform illumination—all weights identical. The array-factor magnitude in dB is presented on two scales. In the upper left a complete hexagonal period of the array factor is presented on a color-coded amplitude scale covering many tens of dB to make the sidelobe structure visible. The superposed hemisphere shows elevation and azimuth as latitude and longitude respectively, assuming that array boresight is towards the horizon. Below that a view magnified in both beamspace and amplitude is presented to make any internal beam structure clearly visible. Each of those 2D plots has the array-factor magnitude along a slice extending rightward from boresight (center) shown as a conventional line plot on its right. On the magnified bottom plots those points 3 dB down from the array-factor peak are flagged in magenta.

2.2 Linear FM

2.2.1 The separable, rectangle case—Extending the 1D FM chirp of Section 1.1 to a rectangle in two spatial dimensions is straightforward. For simplicity we defer spatial sampling at the element positions and consider 2D array-plane position vector $\mathbf{x}$ to be continuously valued. We don't wish to get into issues of array orientation, etc., so here we simply assume the rectangle is aligned with the two axes of $\mathbf{x}$. Beamwidth and time-extent matrices $\mathbf{W}$ and $\mathbf{T}$ are diagonal with positive diagonal elements:

$$h(\mathbf{x}) = \begin{cases} \mathrm{e}^{j\pi\mathbf{x}^{\mathrm{T}}\mathbf{W}\mathbf{T}^{-1}\mathbf{x}} & \text{for } \mathbf{T}^{-1}\mathbf{x} \in \mathcal{S}, \\ 0 & \text{otherwise.} \end{cases} \tag{1}$$

Here set $\mathcal{S}$ is a 1×1 square centered on the origin. In 2D the instantaneous (really "instanspaceous" since $\mathbf{x}$ is a position, but we lack such a word) frequency of a signal $\mathrm{e}^{\mathrm{j}\theta(\mathbf{x})}$ is just $\frac{1}{2\pi}\nabla\theta(\mathbf{x})$, with the gradient taken with respect to position vector $\mathbf{x}$. The phase of signal $h(\mathbf{x})$ of (1) has the parabolic "bowl" shape $\pi\mathbf{x}^{\mathrm{T}}\mathbf{W}\mathbf{T}^{-1}\mathbf{x}$ and instantaneous frequency $\mathbf{W}\mathbf{T}^{-1}\mathbf{x}$. If for simplicity we denote instantaneous frequency by two-vector $\mathbf{k}$ in hopes that it will approximate the 2D Fourier transform's spatial-frequency variable as well and therefore ultimately be the array-plane component of wavenumber for plane waves, we see that this instantaneous frequency ranges over $\mathbf{k} \in \mathbf{W}\mathcal{S}$ or, equivalently, across those

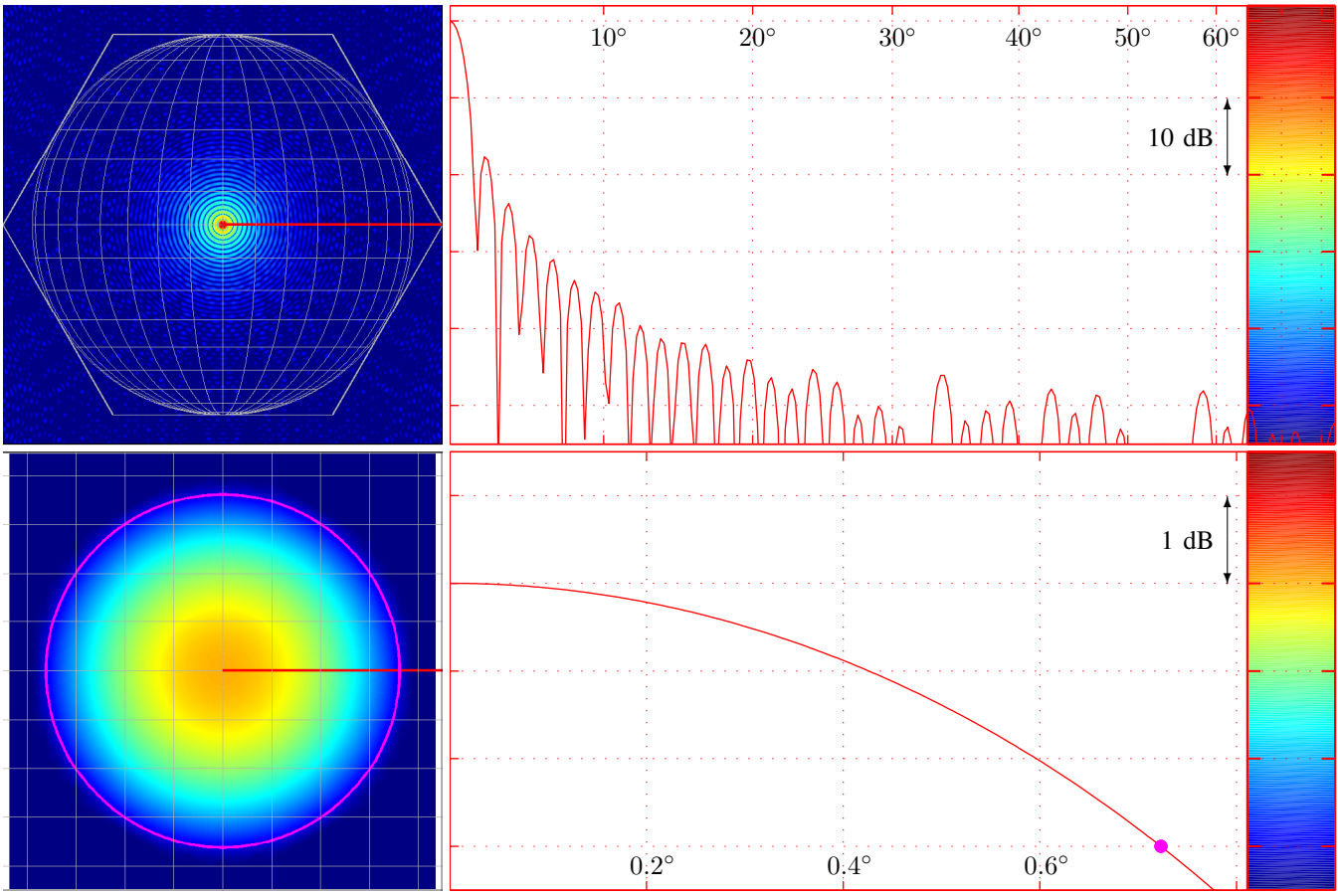

Figure 1 - Uniform weighting.

$\mathbf{k}$ for which $\mathbf{W}^{-1}\mathbf{k} \in \mathcal{S}$. Using $d\mathbf{k}$ and $d\mathbf{x}$ to denote differential areas, $d\mathbf{k}/d\mathbf{x} = |\det(\mathbf{W}\mathbf{T}^{-1})|$, a constant because $\mathbf{k}$ is linear in $\mathbf{x}$. Each realized value of $\mathbf{k}$ is realized for one $\mathbf{x}$ value only, so the Fourier spectrum is roughly constant over the range of $\mathbf{k}$. Indeed, when matrix $\mathbf{WT}$ has large diagonal elements and once again using $\mathbf{k}$ as the transform variable,

$$|H(\mathbf{k})| \approx \begin{cases} \text{some constant} & \text{for } \mathbf{W}^{-1}\mathbf{k} \in \mathcal{S}, \\ 0 & \text{otherwise.} \end{cases}$$

This continuous phase-only taper has a rectangular outline and gives an approximately rectangular beam in spatial frequency $\mathbf{k}$ (sine space).

2.2.2 Elliptical arrays and beams—For an array outline elliptical in vector $\mathbf{x}$ we could use

$$h(\mathbf{x}) = \begin{cases} \mathrm{e}^{\mathrm{j}\pi\mathbf{x}^{\mathrm{T}}\mathbf{W}\mathbf{T}^{-1}\mathbf{x}} & \text{for } \mathbf{x}^{\mathrm{T}}\mathbf{T}^{-2}\mathbf{x} < \frac{1}{4}, \\ 0 & \text{otherwise,} \end{cases}$$

where 2×2 symmetric time and beamwidth matrices $\mathbf{T}$ and $\mathbf{W}$ here are positive definite. The major and minor diameters of the taper are given by the eigenvalues of $\mathbf{T}$. The instantaneous spatial-frequency vector here is again $\mathbf{k} = \mathbf{W}\mathbf{T}^{-1}\mathbf{x}$, and in the ellipse where $h(\mathbf{x})$ is nonzero it ranges over the ellipse in $\mathbf{k}$ for which $\mathbf{k}^{\mathrm{T}}\mathbf{W}^{-2}\mathbf{k} < 1/4$, so

$$|H(\mathbf{k})| \approx \begin{cases} \text{some constant} & \text{for } \mathbf{k}^{\mathrm{T}}\mathbf{W}^{-2}\mathbf{k} < \frac{1}{4}, \\ 0 & \text{otherwise.} \end{cases}$$

resulting in an elliptical beam with major and minor diameters given by the eigenvalues of $\mathbf{W}$.

Any of these continuous-space functions can be sampled spatially to obtain element weights for an array. The primary problem with such "FM beams" is that the approximation error is a function of the (eigenvalues of the) space-beamwidth product $\mathbf{WT}$, which (eigenvalues) must (all) be large. This approximation is not actually reasonable for even the largest actual radar arrays—it would take hundreds of thousand elements to get down to a few dB of ripple—so with (each eigenvalue of) $\mathbf{WT}$ rather small we are reduced to tweaking parameters in hopes of "lucking into" a decent array factor.

2.2.3 Circular-array, circular-beam example designs—We illustrate with circular-array, circular-beam designs by setting $\mathbf{W}$ and $\mathbf{T}$ to scaled identity matrices. The discussion on array geometry in Section 1 gives us $\mathbf{T} = 2\sqrt{1237/3}\,\lambda\mathbf{I}$, and we can parameterize product $\mathbf{WT}^{-1}$ as $\beta\mathbf{I}$ using a scalar parameter β, leaving beamwidth matrix $\mathbf{W}$ implied:

$$h_{\mathbf{x}} = \begin{cases} \mathrm{e}^{\mathrm{j}\pi\beta\|\mathbf{x}\|^2} & \text{for } \|\mathbf{x}\| \le \sqrt{1237/3}\,\lambda, \\ 0 & \text{otherwise.} \end{cases} \tag{2}$$

Figure 3 presents, in its upper and lower halves, the array factors that result for two particular β values. In each 1D plot a horizontal line at 0 dB extends out to the radius of the ideal beam approximated, *i.e.* to the repeated eigenvalue

of matrix $\mathbf{W}$. In the closeups magenta marks the point 4 dB down from the peak (rather than 3 dB as in the other plots).

The boresight array-factor value is especially sensitive to β, most likely due to array-edge effects, so given a desired general range for β, generally one must fine tune β by hand to set this boresight value to something nonextreme relative to the rest of the curve.

In all array-factor plots in this paper there is a dB grid line at the array-factor magnitude maximum, but this level has no other significance. The plots have no particularly meaningful vertical scaling. For actual array-gain calculations for tapers like these, the reader is referred to [19].

2.3 Nonlinear FM, the Gaussian(ish)-beam case

The linear-FM design examples just discussed have instantaneous frequencies that are linear in position $\mathbf{x}$ and so implicitly aim at having their array factors approximate "brick wall" spectra. It is no surprise therefore that nasty array-factor ripples arise as a result, and it certainly seems reasonable to attempt some sort of gradual rolloff as an alternative, in hopes that the approximations will be better, that ripple magnitudes will be significantly lower.

Toward this end, consider the taper

$$h(\mathbf{x}) = \begin{cases} \mathrm{e}^{\mathrm{j}2\sqrt{2\pi}\, r_0 \sigma \left(1 - \mathrm{e}^{-\left(\mathrm{erf}^{-1}(\|\mathbf{x}\|/r_0)\right)^2}\right)} & \text{for } \|\mathbf{x}\| < r_0, \\ 0 & \text{otherwise.} \end{cases} \quad (3)$$

Different authors define the error function with different scalings, but here we use the version implemented by matlab, the odd function defined for positive arguments by

$$y = \mathrm{erf}(x) = \tfrac{2}{\sqrt{\pi}} \int_0^x \mathrm{e}^{-u^2} du. \quad (4)$$

The inverse error function is then defined by $x = \mathrm{erf}^{-1}(y)$ for real arguments having absolute values less than unity. To respect the latter bound, the constant r_0 in (3) must be set greater than the largest value of $\|\mathbf{x}\|$ that will result from sampling, and in our experiments we have generally set it very close to that largest value. Instantaneous frequency

$$\mathbf{k} = \tfrac{1}{2\pi} \nabla \mathrm{phase}(\mathbf{x}) = \tfrac{1}{\|\mathbf{x}\|} \mathbf{x} \sqrt{2\sigma^2}\, \mathrm{erf}^{-1}(\|\mathbf{x}\|/r_0) \quad (5)$$

can be straightforwardly if tediously derived from (3) with many applications of the chain rule using the fairly self-evident relationship $\nabla\|\mathbf{x}\| = \frac{1}{\|\mathbf{x}\|}\mathbf{x}$ and using derivative

$$\tfrac{d}{dy} \mathrm{erf}^{-1}(y) = \tfrac{\sqrt{\pi}}{2} \mathrm{e}^{\left(\mathrm{erf}^{-1}(y)\right)^2}, \quad (6)$$

which is easily worked out from (4). By the development in Section A.2 of the Appendix the Fourier spectrum should take form

$$|H(\mathbf{k})| \propto \frac{\frac{\sqrt{\pi}}{2}\, \mathrm{erf}\left(\|\mathbf{k}\|/\sqrt{2\sigma^2}\right)}{\|\mathbf{k}\|/\sqrt{2\sigma^2}}\, \mathrm{e}^{-\|\mathbf{k}\|^2/(2\sigma^2)}, \quad (7)$$

at least for sufficiently high σr_0, which here serves the role of a time-bandwidth product.

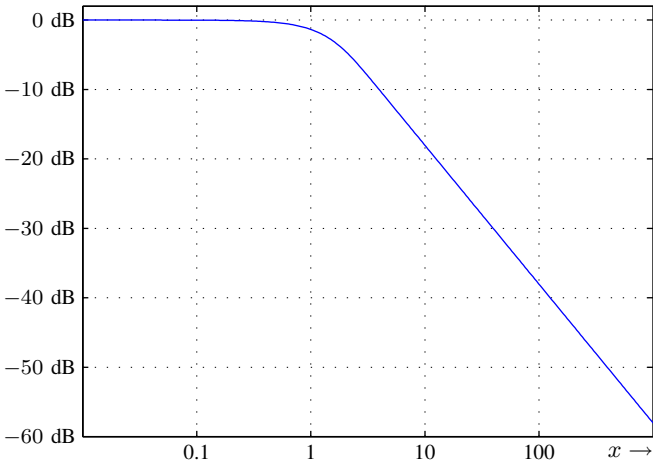

Figure 2 - The "erfinc" function $(\sqrt{\pi}/2)\,\mathrm{erf}(x/\sqrt{2})/(x/\sqrt{2})$.

On the right in (7) the Gaussian rolloff factor $\mathrm{e}^{-\|\mathbf{k}\|^2/(2\sigma^2)}$ is multiplied by the ratio plotted in Fig. 2. That ratio is a sort of "erfinc" function because like the familiar sinc function, it has form $f(x)/x$, has value unity at the origin, and rolls off asymptotically at 20 dB per decade. The Fourier spectrum approximated in (7) then is essentially Gaussian for $\|\mathbf{k}\| < \sigma$ but rolls off somewhat faster than Gaussian for $\|\mathbf{k}\| > \sigma$.

We present specific designs in Fig. 4 for $r_0 = 20.31\lambda$ and two values of σ. The upper, dashed parabolic arc extending downward from 0 dB is the Gaussian rolloff factor $\mathrm{e}^{-\|\mathbf{k}\|^2/(2\sigma^2)}$. The lower, solid parabolic arc below it is the product of that Gaussian rolloff factor and the "erfinc" function in (7) and so represents the spectrum nominally approximated. It is no surprise that the array factor approximates this value more closely when σr_0 is large and that for beam sizes of interest σr_0 in fact is fairly small. Still the resulting array-factor ripple magnitudes can sometimes be made far lower than for the linear-FM tapers by choosing r_0 and σ carefully. Approximation quality is particularly sensitive to σ, and again the value of the array factor at boresight is especially touchy. Small deviations from the σ values shown can triple or quadruple mainbeam dB ripple.

Of note in Fig. 4 are sidelobe levels considerably lower than those typically obtained in local-optimization experiments that begin iterating from uniform illumination.

2.4 Hand shaping an array factor: making a sombrero

In one recent set of experiments [19], we experimented with creating a "sombrero" pattern, one with a relatively narrow beam at a high "top" amplitude and a much wider beam at a lower "brim" amplitude by replacing $\|\mathbf{x}\|$ in (3) with a shaping function $s(\|\mathbf{x}\|)$ to obtain

$$h(\mathbf{x}) = \begin{cases} \mathrm{e}^{\mathrm{j}2\sqrt{2\pi}\, r_0 \sigma \left(1 - \mathrm{e}^{-\left(\mathrm{erf}^{-1}(s(\|\mathbf{x}\|)/r_0)\right)^2}\right)} & \text{for } \|\mathbf{x}\| < r_0, \\ 0 & \text{otherwise.} \end{cases} \quad (8)$$

Figure 5 presents one such design using $s(\|\mathbf{x}\|) = b\|\mathbf{x}\| + (a^m + \|\mathbf{x}\|^m)^{1/m} - a$ with $r_0 = 21\lambda$, $k_0 = 0.3291/\lambda$, $a = 10\lambda$, $b = 0.41$, and $m = 8$. As with the other designs, small changes in any of the five parameters σ, r_0, a, b, or m often result in major changes in the array factor. Trial-and-error exploration of a five-dimensional design space is not particularly easy, yet a few minutes of exploration was sufficient to produce the Figure 5 design.

3. CONCLUSION

The usual instantaneous-frequency approach to creating FM chirps with high time-bandwidth products—basically a stationary-phase approach—was here generalized to phase-only 2D array tapers. Simple computational experiments for a large triangular-grid array then showed that setting taper parameters by trial and error can sometimes be enough to create array factors with at least nonhorrible sidelobe levels and only moderately miserable main-beam ripple levels. We conjecture that such an approach could plausibly be used to initialize a nonlinear weight-optimization process to then improve upon these performance levels by seeking out a local optimum in phase-weight space. Since nonlinear optimization beginning from the usual uniform-weights starting point often leads, in the experiments of other researchers, to much worse sidelobe performance than obtained here, we might reasonably expect the new starting points to improve results substantially.

APPENDIX
RADIAL INSTANTANEOUS FREQUENCY

A.1 The General Case

In the special case of a phase-only taper $h_{\mathbf{x}} = \mathrm{e}^{\,\mathrm{j}\theta(\mathbf{x})}$ having $\theta(\mathbf{x})$ a function of norm $\mathbf{x}$ only, the instantaneous frequency vector is oriented radially and so can be put in the form

$$\mathbf{k} = \mathbf{x}\frac{1}{\|\mathbf{x}\|}g(\|\mathbf{x}\|),$$

a "gain" $g(\|\mathbf{x}\|)$ times a unit vector in the $\mathbf{x}$ direction. If function $g(\ )$ is chosen to be strictly monotonic the map $\mathbf{x} \mapsto \mathbf{k}$ will be invertible on its range: each value of $\mathbf{k}$ will be associated with a single point $\mathbf{x}$, the case in which taking the Fourier spectrum to be approximately proportional to the ratio $d\mathbf{x}/d\mathbf{k}$ of differential areas is plausible. All of this paper's design examples satisfy this condition.

This specific radial structure for the instantaneous frequency implies a corresponding form for differential-area ratio $d\mathbf{x}/d\mathbf{k}$. If we use a radius r and a unit vector $\widehat{u}$ to write $\mathbf{x} = r\,\widehat{u}$,

$$\begin{aligned} \mathbf{k} &= g(r)\,\widehat{u} \\ \|\mathbf{k}\| &= g(r) \qquad \text{(A1)} \\ r &= g^{-1}\big(\|\mathbf{k}\|\big). \qquad \text{(A2)} \end{aligned}$$

In the present 2D case the unit vector takes the form

$$\widehat{u} = \begin{bmatrix} \cos\phi \\ \sin\phi \end{bmatrix},$$

so the differential areas can be be expressed as

$$\begin{aligned} d\mathbf{x} &= r\,dr\,d\phi \\ d\mathbf{k} &= g(r)\,g'(r)\,dr\,d\phi, \end{aligned}$$

using $g'(r)$ for $dg(r)/dr$. Using (A1) and (A2) on the ratio,

$$\frac{d\mathbf{x}}{d\mathbf{k}} = \frac{r}{g(r)\,g'(r)} = \frac{g^{-1}\big(\|\mathbf{k}\|\big)}{\|\mathbf{k}\|\,g'\big(g^{-1}(\|\mathbf{k}\|)\big)}. \qquad \text{(A3)}$$

A.2 A Particular Case

For specific case (5) of instantaneous frequency,

$$\begin{aligned} g(r) &= \sqrt{2\sigma^2}\,\mathrm{erf}^{-1}(r/r_0) \\ g^{-1}(x) &= r_0\,\mathrm{erf}\big(\tfrac{x}{\sqrt{2\sigma^2}}\big) \qquad \text{(A4)} \\ g'(r) &= \tfrac{\sigma}{r_0}\sqrt{\tfrac{\pi}{2}}\,\mathrm{e}^{\left(\mathrm{erf}^{-1}(r/r_0)\right)^2} \qquad \text{(A5)} \\ g'(g^{-1}(x)) &= \tfrac{\sigma}{r_0}\sqrt{\tfrac{\pi}{2}}\,\mathrm{e}^{x^2/(2\sigma^2)}, \qquad \text{(A6)} \end{aligned}$$

where (6) has been used to obtain (A5). Substitution of (A4) and (A6) into (A3) and a little simplification yields

$$\frac{d\mathbf{x}}{d\mathbf{k}} = \frac{2r_0^2}{\pi\sigma^2}\left(\tfrac{\sqrt{2\sigma^2}}{\|\mathbf{k}\|}\,\tfrac{\sqrt{\pi}}{2}\,\mathrm{erf}\big(\tfrac{\|\mathbf{k}\|}{\sqrt{2\sigma^2}}\big)\,\mathrm{e}^{-\|\mathbf{k}\|^2/(2\sigma^2)}\right),$$

where the arrangement of constants is such that the quantity in the outer parentheses goes to unity as $\|\mathbf{k}\|$ goes to zero.

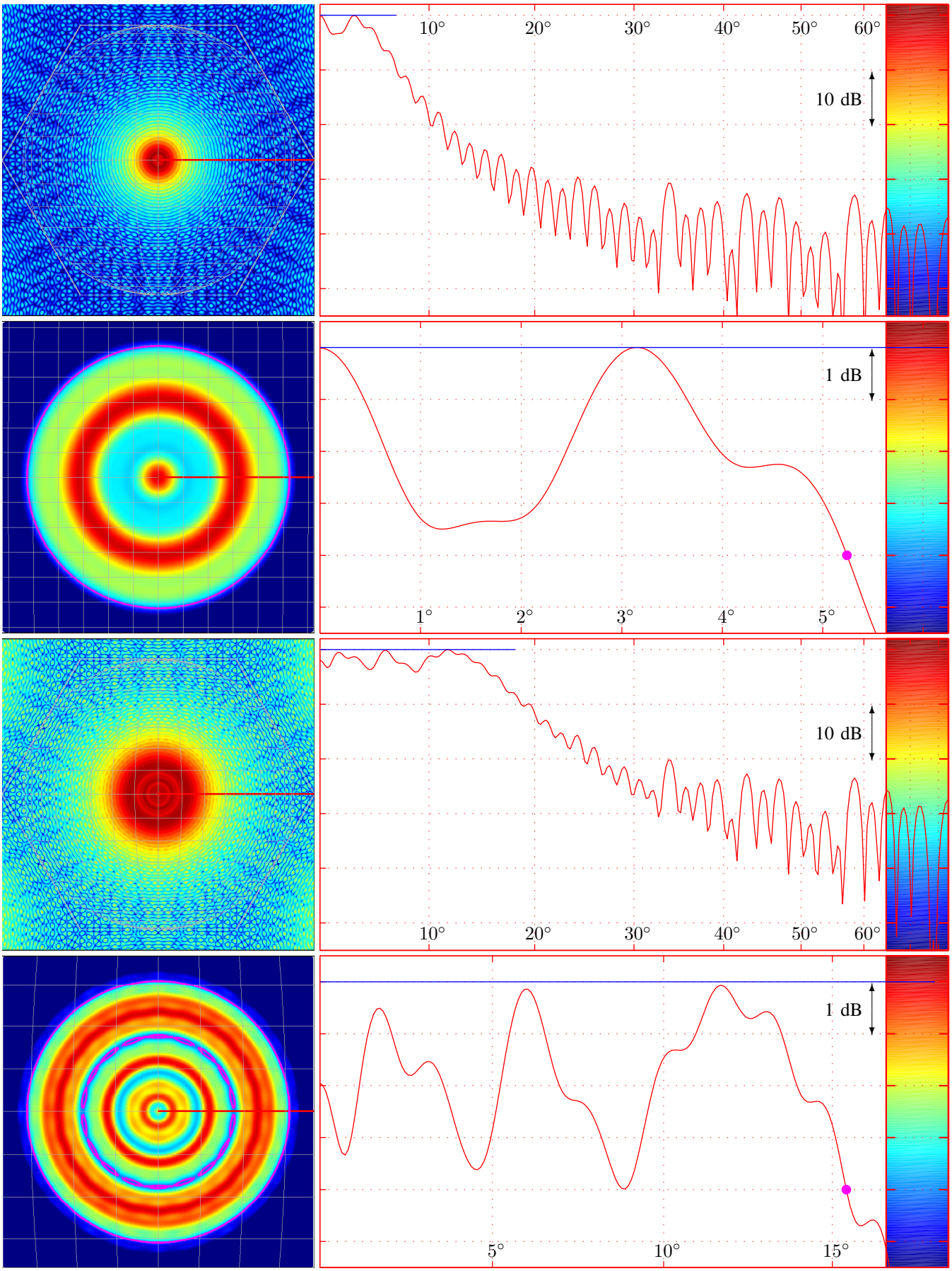

Figure 3 - Linear-FM phase taper of (2) with (top) $\beta = 0.00598/\lambda^2$ and (bottom) $\beta = 0.0153/\lambda^2$.

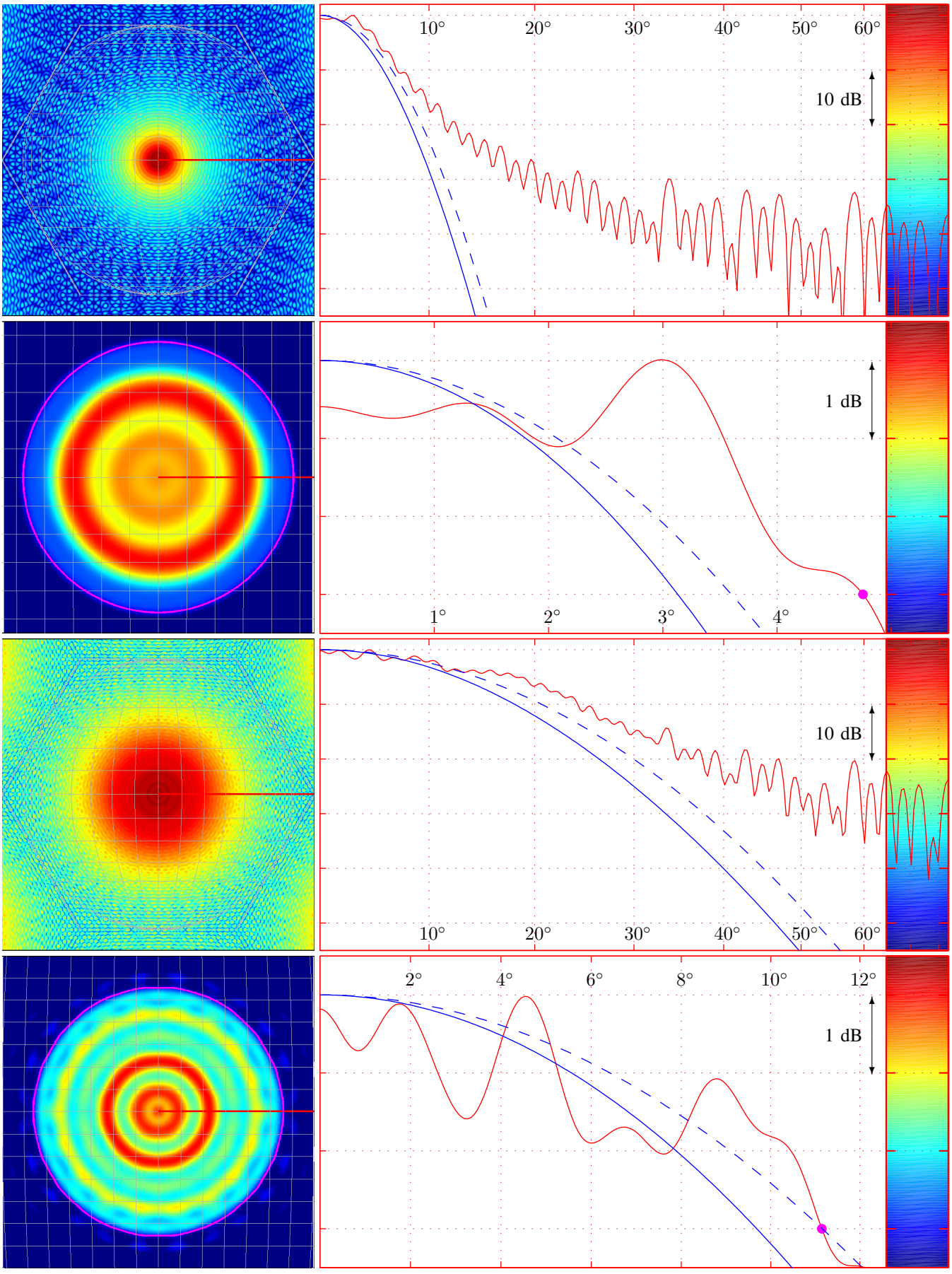

Figure 4 - Gaussian-beam FM taper (3) with $r_0 = 20.31\lambda$ with (top) $\sqrt{2\sigma^2} = 0.1068/\lambda$ and with (bottom) $\sqrt{2\sigma^2} = 0.3291/\lambda$.

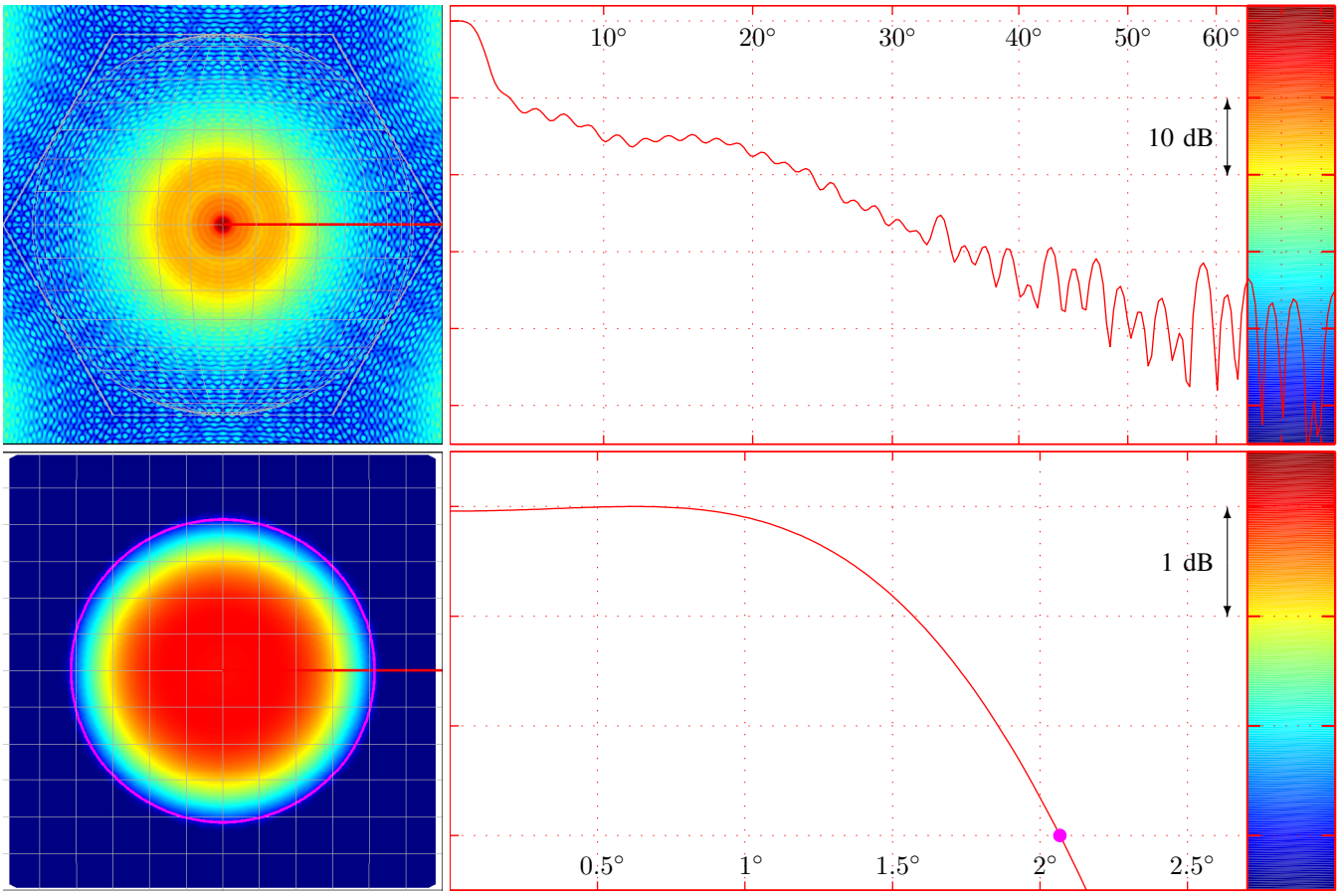

Figure 5 - Sampling (8) to create a phase taper yields a crude "sombrero" array factor.

REFERENCES

[1] D. P. Scholnik and J. O. Coleman, "Optimal array-pattern synthesis for wideband digital transmit arrays," *IEEE J. Selected Topics in Sig. Proc., Special Issue on Convex Optimization Methods for Signal Processing*, vol. 1, no. 4, pp. 660–677, Dec. 2007.

[2] J. F. Sturm, "Using SeDuMi 1.02, a Matlab toolbox for optimization over symmetric cones," *Optimization Methods and Software*, vol. 11–12, pp. 625–653 (vers. 1.02/1.03), 1999, updated for vers. 1.05 online: http://www.optimization-online.org/DB_HTML/2001/10/395.html.

[3] P. Sridevi, G. Raju, and P. Misra, "Effect of digital phase shifters on phase only controlled SLS difference patterns," in *Int'l. Conf. on Electromagnetic Interference and Compatibility*, 1997, pp. 163–166.

[4] R. Kinsey, "Phased array beam spoiling technique," in *IEEE Antennas and Propagation Society Int'l Symp.*, vol. 2, 1997, pp. 698–701.

[5] H. Steyskal, "Simple method for pattern nulling by phase perturbation," *IEEE Trans. Antennas and Propagation*, vol. 31, no. 1, pp. 163–166, 1983.

[6] A. Chakraborty, B. Das, and G. Sanyal, "Beam shaping using nonlinear phase distribution in a uniformly spaced array," *IEEE Trans. Antennas and Propagation*, vol. 30, no. 5, pp. 1031–1034, 1982.

[7] A. S. Dunbar, "On the theory of antenna beam shaping," *J. Applied Physics*, vol. 23, no. 8, pp. 847–853, 1952, http://link.aip.org/link/?JAP/23/847/1.

[8] R. Young, "Antenna pattern control by phase-only weighting," in *IEE Colloquium on Phased Arrays*, 1991, pp. 5/1–5/7.

[9] S. Sun and H. Li, "Simplified beamforming on phase-only arrays," in *Int'l Conf. on Neural Networks and Signal Processing*, vol. 2, 2003, pp. 1290–1293.

[10] A. Khzmalyan and A. Kondratiev, "The phase-only shaping and adaptive nulling of an amplitude pattern," *IEEE Trans. Antennas and Propagation*, vol. 51, no. 2, pp. 264–272, 2003.

[11] D. Chang, C. Hung, C. Hu, K. Ho, and H. Chen, "Synthesis of array antenna with broad nulls," in *Asia-Pacific Microwave Conf.*, vol. 1, 1993, pp. 88–92.

[12] E. Dufort, "Pattern synthesis based on adaptive array theory," *IEEE Trans. Antennas and Prop.*, vol. 37, no. 8, pp. 1011–1018, 1989.

[13] R. Voges and J. Butler, "Phase optimization of antenna array gain with constrained amplitude excitation," *IEEE Trans. Antennas and Propagation*, vol. 20, no. 4, pp. 432–436, 1972.

[14] G. Brown, J. Kerce, and M. Mitchell, "Extreme beam broadening using phase only pattern synthesis," in *IEEE Workshop on Sensor Array and Multichannel Processing*, 2006, pp. 36–39.

[15] O. Bucci, G. D'Etia, and G. Romito, "Optimal synthesis of reconfigurable conformal arrays with phase only control," in *IEEE Antennas and Propagation Society Int'l Symp.*, vol. 2, 1996, pp. 810–813.

[16] A. Trastoy, F. Ares, and E. Moreno, "Phase-only control of antenna sum and shaped patterns through null perturbation," *IEEE Antennas and Propagation Magazine*, vol. 43, no. 6, pp. 45–54, 2001.

[17] L. Marcaccioli, R. V. Gatti, and R. Sorrentino, "Series expansion method for phase-only shaped beam synthesis and adaptive nulling," *URSI Int'l Symp. Electromagnetic Theory*, 2004.

[18] E. Fowle, "The design of FM pulse compression signals," *IEEE Trans. Information Theory*, vol. 10, no. 1, pp. 61–67, 1964.

[19] K. R. McPhail, J. O. Coleman, and D. P. Scholnik, "Experiments in weight design for a sombrero array pattern," Naval Research Laboratory, NRL Memo Report 9232, sometime in early 2010.